# A numerical study of dust explosion properties of Hydrogen storage alloy materials

**W Malalasekera[1], B Liu[1], Salah Ibrahim[2] and A R Uyanwaththa[1]**

**Abstract.** Hydrogen as a clean fuel has gained increased attention in the recent years and considerable research is being undertaken to develop hydrogen storage technologies. Hydrogen storage using metal hydride is one such technology. Hydride materials, used in hydrogen storage technologies, in powder form can be an explosion hazard and testing these materials using standard techniques is also difficult. Research reported in this paper is an attempt to develop numerical methods to obtain explosion properties of such materials. In this work a one dimensional transport-type model is presented to simulate the dust explosion process in a closed 20-L spherical vessel. Transport equations for energy, species and particle volume fraction are solved with the finite difference method, whilst velocity distribution and pressure are updated with numerical integration of the continuity equation. The model is first validated with experimental data and then applied to simulate the explosion process of an AB2-type alloy powder used for hydrogen storage. Two kinetic models accounting for the particle burning mechanism are investigated in the current study. One is based on an Arrhenius surface reaction law, the other is based on a simplified diffusion-type $d_2$ law. The former is found to be better in terms of prediction of the deflagration indices. This work is of great significance in safety assessment of new hydrogen storage materials in the processes of their production, storage and transportation. **Key words:** dust explosion; numerical simulation; $AB_2$ alloy; hydrogen storage

## 1. Introduction

Hydrogen is seen as the preferred fuel for the future due to several reasons. The current trend in city air pollution arising from mainly carbon based fuels has to be curtailed to maintain healthy living environments in major cities. With the increase of the availability of renewable electricity capacity, energy storage capabilities are required to store excess electricity which can be intermittent. In European countries there is also a drive de-carbonize the gas network where Hydrogen could be injected into the gas networks. In this context Hydrogen is being recognized as a future energy carrier to substitute the fossil fuels due to its high energy density, possible future availability and excellent eco-friendliness in the era of growing threats of global warming and energy crisis. A hydrogen economy is one in which hydrogen and electricity can theoretically satisfy the whole energy demand [1]. Besides hydrogen can be derived through a variety of ways from renewable energy resources [2]. The storage and transportation of the hydrogen plays a vital role in setting up a hydrogen-based energy system [3–8]. Among the existing means of hydrogen storage, high-pressure gaseous and cryogenically cooled liquid hydrogen forms the majority of capacity. However, the shortcomings of these technologies such as low energy density by mass, unsuitability for mobile applications, high cost of preparation (compression and liquefaction) and concerns for public safety prohibit large-scale applications in the future hydrogen economy [9]. Alternatively, metal hydride is an ideal hydrogen

[1] Mechanical, Electrical and Manufacturing Engineering, , Loughborough University, Leicestershire, UK
[2] Aeronautical and Automotive Engineering, Loughborough University, Leicestershire, UK

storage media with relatively high hydrogen storage capacity, moderate hydrogenation/ dehydrogenation temperature and pressure, and moreover inherently safer than compressed gas and cryogenic liquid [1]. Despite of the relatively low gravimetric hydrogen storage capacity at room temperature, metal hydride can provide a superior volumetric hydrogen density which is even higher than liquid hydrogen [10,11]. In the past several decades, tremendous efforts have been put into the study of metal hydride for hydrogen storage. Results obtained have been encouraging [12]. Among various metallic candidates, the Zr and Ti-based $AB_2$-type Laves phase alloy have been found to have good attributes for hydrogen storage, such as relatively high capacity, good kinetics, long life cycle and low cost of production, etc. [7,13–16] In order to increase the efficiency of hydrogenation and dehydrogenation, the alloy products usually undergoes a post-processing ball-milling operations to increase the specific surface area therefore the metal hydrides are used in the form of particulates. As a consequence, a flammable metal dust cloud can be potentially formed due to a leakage of the metal powder during the process of its production, transportation, storage and utilization, which can be a significant explosion risk. Accidental dust explosions have been recognized as a great industrial hazard for a long time [17]. In the development of hydrogen storage technologies using metal hydrides, it is essential to assess the dust explosion risks associated with the storage materials. In assessing dust explosion hazards of materials the usual practice is to conduct standard tests such as Minimum ignition energy (MIE), Minimum ignition temperature in cloud (MIT cloud), Minimum ignition temperature in layer (MIT layer), Minimum explosible concentration (MEC), Limiting oxygen concentration for combustion (LOC) and most importantly explosion severity tests ($K_{st}$, $P_{max}$), in 20L and $1m^3$ vessels. Depending on the results of these tests the material could be classified and required safety measures could be used to mitigate explosion hazard. However, metal hydrides used for hydrogen storage pose an added complication, i.e. most hydrogen storage metal hydrides are flammable and pyrophoric. Hence standard tests could not be performed to obtain explosion characteristics. The research reported in this paper attempts to address this problem by developing a numerical simulation methodology to obtain important data for metal hydride powders.

Modelling and numerical simulation of metal dust combustion/explosions is a very complex task. The major problems are defining cloud structure, properties and mechanisms involved in combustion. Despite great challenges due to lack of effective methods to describe the dust cloud structures and related flame propagation models [18], a number of numerical models have been developed to simulate this process. Since the combustion mechanism of a flammable particulate suspension in air, is highly dependent on the fuel species, particle properties and the way that the suspension has been formed, it is difficult to develop a general model to simulate this process. Seth [19] proposed a mathematical model to describe the flame propagation of hydrogen carbon spray in a closed volume by solving 1D transport equations of energy and mass. In this model, liquid droplets and air were considered separately as two continuous phases based on the Eulerain framework, and combustion reactions were assumed to be restricted within the gaseous phase where vaporized fuel emitted from the liquid droplet was mixed perfectly with air. Subsequently, Aggarwal [20] modified this model such that the liquid droplet was considered as a discrete phase using the Lagrangian approach. Continillo [21] adapted Aggarwal's model to a 1D spherical co-ordinate system and then simulated explosions occurred in a closed sphere. These inspiring spray explosion models were have been straightforwardly applied to simulate explosions caused by solid dust of some organic substances, since the combustion mechanisms are quite similar [22]. Di Benedetto [23,24] assumed that homogeneous gas phase combustion was the rate-controlling step in organic dust explosions with low particle diameters such as corn starch, poly-ethylene and cellulose. They developed a model based on the above assumption and finally estimated the speed of flame propagation using Chemkin software. Similar to the organic materials, metal can also form detonable dust cloud when mixed with oxidizer and is more dangerous due to high calorific value. Metal dust explosions have also been a research concern to the combustion community for many years [25].

The aim of this study is to develop a numerical model to simulate the explosion process of the flammable suspension of the $AB_2$-type hydrogen storage alloy – $(Ti_{0.65}Zr_{0.36})_{1.05}Mn_{0.96}Cr_{0.81}Fe_{0.22}$ in air, and then to calculate the values of $P_{max}$ and $K_{st}$ at different conditions, by which a safety assessment can be made to guide the production process of this metal powder. The first part of this study forms

the main content of the current paper focusing on the development and validation of the numerical model. A detailed safety analysis of the alloy dust explosion will be presented in future publications.

## 2. Methodology

*2.1 Governing equations*

The explosion severity of a dust cloud is generally quantified with the maximum pressure rise, Pmax and the deflagration index, $K_{st}=(dp/dt)_{max}\cdot V^{1/3}$ which represents the maximum pressure rise rate during the explosion. These parameters can be measured in a standard 20L apparatus [25,26] in accordance with an international standard ISO 6184-1 [27]. The testing chamber is a hollow sphere with a centre igniter and a particle distributor. Solid sample is stored in a high-pressure container and injected into the pre-evacuated chamber through the distributor at the beginning of the test. Igniter is then triggered to ignite the dust cloud after a short delay to allow sufficient dispersion. During the whole process of the explosion, overpressure generated can be recorded by a pressure sensor and hence the time evolution of the internal pressure can be obtained. The most straightforward way to reproduce this process numerically is to develop a one dimensional model based on a spherical symmetric co-ordinates to simulate the flame propagation with appropriate boundary conditions. Considering the fact that key properties of the flame may be evenly distributed in concentric spheres, it is safe to reduce a complex three-dimensional phenomenon into a simple one-dimensional process with necessary assumptions. Radial pressure gradient is neglected due to low Mach number of the flow, hence the pressure is assumed to be spatially uniform. Gas phase is assumed to obey the ideal gas law and the effect of solid phase is ignored as the solid volume fraction is fairly small. Viscous dissipation is neglected and the kinetic energy of the flow is negligible compared with its thermal energy. Specific heats of the species are assumed to be constant during the explosion. Mass diffusivities of each pair of species are assumed to be equal. Lewis Number is assumed to be unity.

The gas phase continuity under spherical co-ordinate is given by Equation (1). No source terms appear on the right hand side of this equation, as the metal oxide produced is assumed to remain a solid form and the gaseous product originated from thermal dissociation of the solid oxide is also neglected.

$$\frac{\partial \rho}{\partial t}+\frac{1}{r^2}\frac{\partial}{\partial r}\left(r^2\rho u\right)=0 \tag{1}$$

Where $\rho$ is the gas density ($kg\cdot m^{-3}$), $t$ the time (s), $r$ the radial distance (m) and $u$ is the gas phase velocity ($m\cdot s^{-1}$).

For simplicity, air is assumed to be composed of 78% nitrogen and 22% oxygen by volume throughout this study. Thus, only one species transport equation needs to be solved for the gas phase to account for the consumption of oxygen during the explosion. Nitrogen is assumed to be completely inert and the mass fraction can be obtained directly through (1-wt.% of oxygen). Species transport equation for oxygen is given by Equation (2). By subtracting Equation (1)$\cdot Y_{O2}$ from Equation (2), a simplified form of the species equation of oxygen is obtained, given by Equation (3).

$$\frac{\partial\left(\rho Y_{O_2}\right)}{\partial t}+\frac{1}{r^2}\frac{\partial}{\partial r}\left(r^2\rho u Y_{O_2}\right)=\frac{1}{r^2}\frac{\partial}{\partial r}\left[r^2\rho(D+D_t)\frac{\partial Y_{O_2}}{\partial r}\right]-\Re_{O_2} \tag{2}$$

$$\rho\frac{\partial Y_{O_2}}{\partial t}+\rho u\frac{\partial Y_{O_2}}{\partial r}=\frac{1}{r^2}\frac{\partial}{\partial r}\left[r^2\rho(D+D_t)\frac{\partial Y_{O_2}}{\partial r}\right]-\Re_{O_2} \tag{3}$$

where $Y_{O_2}$ is the mass faction of oxygen ($kg\cdot kg^{-1}$), $D$ and $D_t$ are the binary molecular and turbulent diffusion coefficients, respectively ($m^2s^{-1}$), $\Re_{O_2}$ the net mass consumption rate of oxygen ($kg\cdot m^{-3}\cdot s^{-1}$). $D_t$ is assumed to be a constant ranging from 0.001 to 0.01 in this study, which correspondingly represents a certain amount of turbulence effect and can be determined using the Prandtl mixing

theory [28]. The mass consumption rate of oxygen is in a stoichiometric relation to the combustion rate of the metal particle $\dot{\omega}$.

Similar to the species equation, a simplified gas phase energy equation can be obtained by from the original transport equation of energy, given by Equation(4). It should be noted that since the Lewis number is assumed to be unity, thermal diffusivity is then identical to the mass diffusivity.

$$\rho\frac{\partial T}{\partial t}+\rho u\frac{\partial T}{\partial r}=\frac{1}{r^2}\frac{\partial}{\partial r}\left[r^2\rho(D+D_t)\frac{\partial T}{\partial r}\right]+\frac{1}{C_p}\left(\frac{dp}{dt}+\dot{\omega}\Delta h_r f\right) \tag{4}$$

where $T$ the temperature (K), $C_p$ the specific heat of the gas mixture ( $J\cdot kg^{-1}\cdot K^{-1}$) which can be calculated by mass weighed averaging using corresponding values of pure components, $\Delta h_r$ the combustion enthalpy based on per unit mass of the fuel ($J\cdot kg^{-1}$), $f$ a factor to be determined in the simulation to ensure the correct flame temperature. For the sake of simplicity, a full set of solid phase equations are not solved in the current study, thus the gas phase temperature may be overestimated as a consequence of overestimation of the total heat released in the gas phase. In fact, a sub-model should be employed in the future to account for the effects of the endothermic dissociation reactions of the oxide products. At present, the factor $f$ is used in the current explosion model to account for the effects of the aforementioned uncertainties. From a numerical point of view, the pressure gradient term on the right hand side of Equation (4) is undesirable as it is an unknown variable coupled with gas phase temperature and density via the ideal gas equation of state. To decouple the pressure gradient from the energy equation, a new variable is defined as $\varphi=Tp^{(1-\gamma)/\gamma}=Tp^{\Gamma}$ where $\gamma$ is the specific heat ratio. Equation (4) can be rearranged into a new equation about $\varphi$ without a pressure derivative term.

$$\frac{\partial\varphi}{\partial t}+u\frac{\partial\varphi}{\partial r}=\frac{\varphi}{r^2}\frac{\partial}{\partial r}\left[r^2\left(\frac{D+D_t}{\varphi}\right)\frac{\partial\varphi}{\partial r}\right]+\frac{p^{\Gamma}}{\rho C_p}\dot{\omega}\Delta h_r f \tag{5}$$

Since the particle size of the solid phase in a dust cloud is considerably small, velocity of the particles can be assumed to be the same as the local gas phase velocity. In other words, the solid phase is fully carried by the gas phase. This simplification will not cause significant errors considering the fact that the explosion occurs within a closed volume so that the magnitude of the main flow velocity is not expected to be very high due to spatial confinement. The mass diffusion of the solid particles is also neglected due to high particle density. A governing equation of the solid volume fraction is then written immediately as follows.

$$\frac{\partial X}{\partial t}+\frac{1}{r^2}\frac{\partial}{\partial r}\left(r^2uX\right)=-\frac{\dot{\omega}}{\rho_p} \tag{6}$$

The above transport equations are solved sequentially to gain the corresponding variables of interest such as the species mass faction, the gas phase temperature, and the volume fraction of the solid phase. With these results, the velocity field and the gas phase pressure can be determined afterwards. The following equation for radial velocity distribution is obtained immediately by integrating Equation (1) over (0, r).

$$u(r)=-\frac{1}{\rho r^2}\int_0^r r^2\frac{\partial\rho}{\partial t}dr \tag{7}$$

Further, by applying the velocity boundary condition at the wall of the sphere $u_R=0$ to Equation (7), the following equation is obtained.

$$\int_0^R r^2\frac{\partial\rho}{\partial t}dr=0 \tag{8}$$

Pressure update can be finally achieved by substituting the ideal gas equation of state $p = \rho R_g T / w_{av}$ into Equation (8) to yield Equation (9). Mean molecular weight of the gas phase required in Equation (9) is calculated via $w_{av} = 1/\sum_i \left(Y_i / w_i\right)$ which has been determined through species equations in a previous step. Equation (2) is then written in a temporal discrete form to calculate pressure of the current time step using the information from the previous time step. Gas phase density is then updated through the ideal gas equation of state with updated pressure. Velocity distributions of the gas phase is then calculated through Equation (7).

$$\int_0^R r^2 \frac{\partial \rho}{\partial t}\left(\frac{p w_{av}}{R_g T}\right) dr = 0 \tag{9}$$

*2.2 Combustion models*

In this paper, two candidate kinetic models, namely kinetic I and kinetic II, describing single spherical particle combustion are investigated and results obtained are compared against experimental data to find out which one is more suitable to describe the explosion process. Kinetic model I is formulated based on a surface reaction mechanism of [29], where combustion rate is calculated by Equation (10).

$$\dot{\omega} = 3 k R_p X \frac{w_p w_{av}}{w_{O_2}} p Y_{O_2} \tag{10}$$

Where $k$ is the rate factor estimated by the Arrhenius law $k = A\exp(-E/R_g T)$, $R_p$ the mean particle radius (m), $X$ the volume fraction of the metal particles, $w_p$ and $w_{O_2}$ are molecular weights of the solid metal and oxygen, respectively, $w_{av}$ is the average molecular weight of the gas phase(kg·kmol$^{-1}$), $p$ the pressure (Pa), $Y_{O_2}$ the mass fraction of oxygen.

Kinetic II is a simplified d$^2$-type combustion law given by [30]. In this paper, the effect of the internal convection of the particle on the mass transfer rate (i.e. combustion rate) is ignored. The single particle combustion rate is then given by Equation (11).

$$\dot{\omega} = \frac{3 X \rho_p}{\tau} \tag{11}$$

where $\tau$ is a characteristic burning time of the single particle measured by experiments, which is related to particle life time and can be calculated by Equation (12).

$$\tau = K \frac{4 R_p^2}{Y_{O_2}^{0.9}} \tag{12}$$

where $K$ is a burning rate constant. A problem of kinetic II is the particle ignition. Different from kinetic I in which the minimum temperature required for the particle starts to burn is determined by the frequency factor and the activation energy through the Arrhenius law, no ignition temperature criterion is implied in kinetic II. Hence, an ignition temperature needs to be specified as the ignition criterion, indicating that no combustion happens when the temperature is lower than this ignition temperature. Then, the complete mechanism can be written in the following form,

$$\dot{\omega} = \begin{cases} \dfrac{3X\rho_p Y_{O_2}^{0.9}}{4KR_p^2} & T \geq T_{ig} \\ 0 & T \leq T_{ig} \end{cases} \tag{13}$$

*2.3 Initial and boundary conditions*

Apart from the explosion severity (measured by $P_{\max}$ and $K_{st}$), explosion sensitivity is also of great importance in risk assessment of a flammable dust cloud. In general, explosion sensitivity can be measured by three parameters which are the minimum ignition temperature (MIT), minimum ignition energy (MIE) and lower explosion limit (LEL), respectively. Technically, these parameters can be estimated with a parametric study implemented in the current explosion model. However, the anticipated prediction may be not be accurate, since the real physics of ignition is extremely complex, for example, the coated inert oxide on the surface of the metal particles significantly increases the ignition energy threshold, which is not considered in the current model. An ignition sub-model will be developed in the future to account for the complex ignition kinetics. Although the prediction of explosion sensitivity is not performed in the current study, a suitable ignition method is still required in order to start the explosion numerically. Two numerical ignition methods are used in this study and found to be approximately equivalent in propagating a flame. First method is to specify an ignition energy density which is evenly distributed in a spherical region with a radius of 1mm at the centre of the 20L-vessel, see Figure 1. In this method, an energy source term is directly added to the energy equation and lasts a short period of time (e.g. 15 time steps) to simulate an instantaneous high-energy ignition source. The other method is to specify a high initial temperature field (2500K) within the ignition zone and reduce the initial concentration of fuel and oxidizer accordingly to simulate the early stage of the explosion right after ignition.

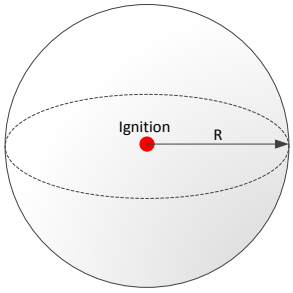


Figure 1: Schematic of ignition in the 20L-vessel

For initial conditions of the model, at $t = 0$, pressure is set to be the atmosphere pressure of 1atm. Initial field of $\varphi$ for the energy equation is calculated from the initial temperature field through relation $\varphi_0 = T_0 p_0^{\Gamma}$ where temperature depends on the ignition method used in an individual simulation run. For ignition method I, the initial temperature is evenly distributed in the whole domain with a constant value of 298K, whereas for ignition method II, temperature takes a value (e.g. 2500K) within the ignition zone and 298K elsewhere. Initial mass fractions of the gas mixture are given based on air at a thermodynamic standard state. Initial volume fraction of the metal particles varies correspondingly with the equivalence ratio investigated in each individual simulation run. Both the solid and gas are assumed to be static before ignition, therefore the initial main flow velocity is 0 throughout the whole domain.

For boundary conditions, the wall of the 20L-vessel is assumed to be impermeable and adiabatic. Hence, no heat and mass loss is considered at wall. A homogeneous Neumann boundary condition is used for energy and species equation accordingly, i.e. $\left(\partial\phi/\partial r\right)_R = 0$, $\left(\partial Y_{O_2}/\partial r\right)_R = 0$.

Since no mass loss of the solid particles at wall, the homogeneous Neumann condition is also applicable for the governing equation of solid volume fraction, i.e. $\left(\partial X / \partial r\right)_R = 0$. For boundary conditions at the ignition point, symmetry conditions are used for all variables.

**3. Numerical simulation**

Governing equations (3), (5) and (6) are solved by an implicit finite difference method. Fine temporal and spatial step sizes are used to guarantee a good accuracy of the solution. Table 1 gives the details of the numerical strategy used in the simulation.

Table 1 Numerical strategy

| Parameter | Value/method |
|---|---|
| Radius of the domain R (mm) | 168 |
| Spatial step size $\Delta r$ (mm) | 0.25 |
| Temporal step size $\Delta t$ (s) | $1 \times 10^{-7}$ |
| Spatial discretization scheme | $2^{nd}$ order central differencing |
| Linear solver | TDMA |

Once the governing equations are solved, temperature can be recovered from the $\varphi$ field. It should be noted that the pressure used in temperature recovery is taken from the previous iteration. Then, pressure, velocity are updated with numerical integrations in the whole domain according to corresponding methods described above. Density and molecular weight of the gas phase are also updated appropriately during this process. An iteration loop is finished when all variables are updated once. The loop will be conducted once again if convergence has not been achieved. The maximum number of iteration of each time step is set to 10 which is found to be sufficient to achieve convergence.

**4. Results and discussion**

*4.1. Flame properties*

The numerical model depicted in the above section is implemented through an in-house Fortran code named DUST. Spatial distributions of the key variables are plotted at intervals of several milliseconds to show the properties of a propagating flame during the explosion process, which are presented in Fig. 2 (a) - (f). Since the ignition method has no significant effect on the prediction of the main parameters interested in this work, all the simulation results presented in this article are obtained with ignition method II. Nevertheless, it should be noted that the ignition method does have some effects on the temperature profile within the ignition zone especially at the early stage of the explosion, which can been seen clearly in Fig.2 (a) that an overheated core appears at the centre with a radius of about 5mm at 2ms of the explosion. This may be caused by an overestimated heat release in this zone when using ignition method II to trigger the explosion. In ignition method II, the high ignition temperature is assumed to be achieved by burning out a certain amount of the fuel in the ignition zone so that the fuel remained therein should be lower than that of the unburned mixture elsewhere in the chamber. Since it is difficult to know how much fuel is consumed to produce a pre-assigned ignition temperature, values are roughly estimated as 0.1 for oxygen mass fraction and 0.05 for volume fraction of the fuel, respectively. Despite this, the mis-prediction of temperature profile only restricted to a small volume at the centre of the chamber, which almost has no effects on the overall thermal characteristic and pressure rise. It can also be noted from Fig.2 (a) that temperatures of both the burned and unburned gas increase with the propagation of the flame during the explosion process, which can be attributed to significant pressure rise due to full confinement of the explosion chamber.

Fig.2 (b) shows the result of gas density evolution in the explosion process. A large density difference can be observed between the cold side (unburned gas side) and the hot side (burned gas side) of the flame. In the first 2/3 of the explosion in terms of radial distance of the flame position, the density difference changes are insignificant, whereas in the last 1/3 of the explosion, a steep increase is observed which can be attributed to a sharp compression of the unburned gas in a relatively short distance. The large density difference is intrinsically related to large temperature difference of the

burned gas and unburned gas. Hence, it tends to vanish at the end of the explosion when the whole chamber is occupied by burned gas only.

The velocity profiles obtained from the simulation are shown in Fig.2 (c). It can be observed from Fig.2 (c) that the directions of the gas velocity are opposite on the two sides of the flame. They are both in an outward direction when observing from the centre of the flame. In the first 2/3 of the explosion, positive velocity is significant indicating that the propagation of the flame contributes the most to the overall gas movement. However, in the last 1/3 of the explosion, the gas emission from the flame contributes more due to a slowdown of the flame which can be seen from Fig.3 showing the evolution of the flame speed.

Fig.2 (d), (e) and (f) show the distributions of reaction rate, oxygen mass fraction and fuel volume fraction, respectively. Chemical reactions are restricted within a thin layer of the flame for most of the time during the explosion. However, the reaction zone is slightly broadened near the end of the explosion. For most of the time in the explosion event, solid is excessive. However, when it is close to the end of the explosion, oxygen becomes excessive. This reversal may have caused the broadening of the flame, which can be observed from Fig 2(d)) It can be explained more reasonably by Fig.2 (e) and (f), from which we can see solid particles are not burned out in the flame zone before 30ms whereas the oxygen is consumed completely. This can be attributed to the thermal expansion which causes a significant decrease in gas density within the flame zone whilst the volume fraction of the particles is not affected. As a result, the available mass of oxygen for combustion decreases. The situation is reversed when the pressure increases to a very high value near the end of the explosion that the gas density in the flame zone increase dramatically due to compression. Gas density in the reaction zone increases sharply due to sharp pressure rise, which allow more oxygen to react with the solid. Near the end of the explosion, oxygen becomes excessive, and solid can be consumed entirely. The former can be referred to as an oxygen controlled process and the latter, on the other hand, can be referred to as a particle controlled process. The reaction changes from the former to the latter during the explosion process and the flame is broadened, which can be seen from the plots of reaction rates in Figure 2(d).

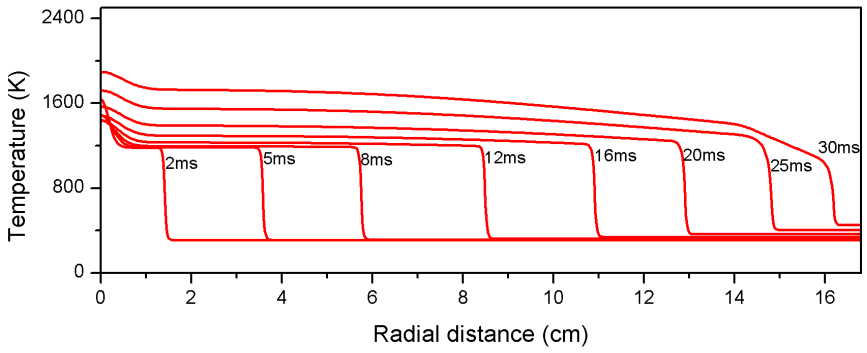


(a)

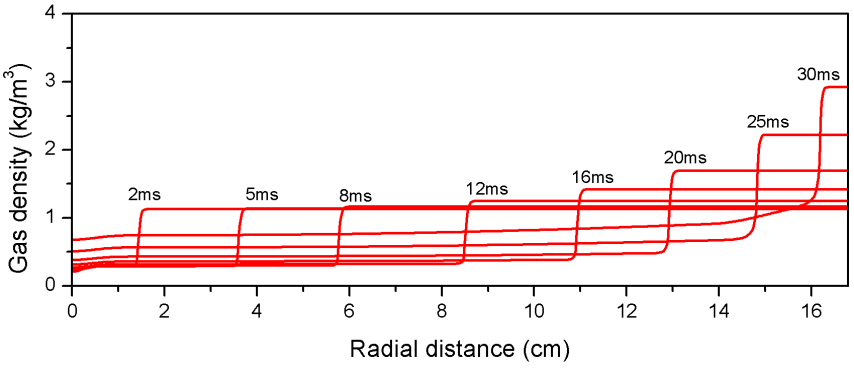


(b)

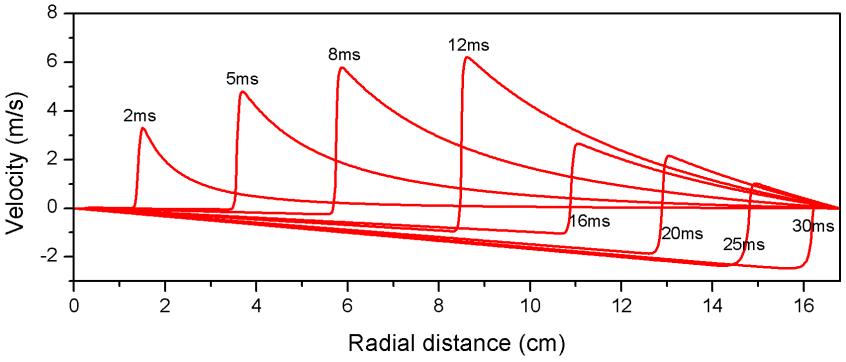


(c)

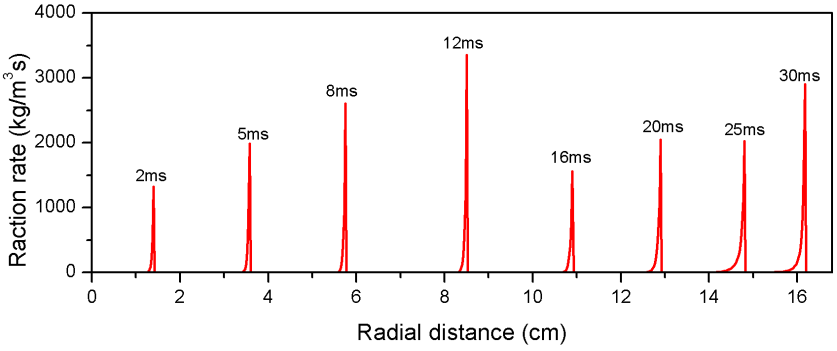


(d)

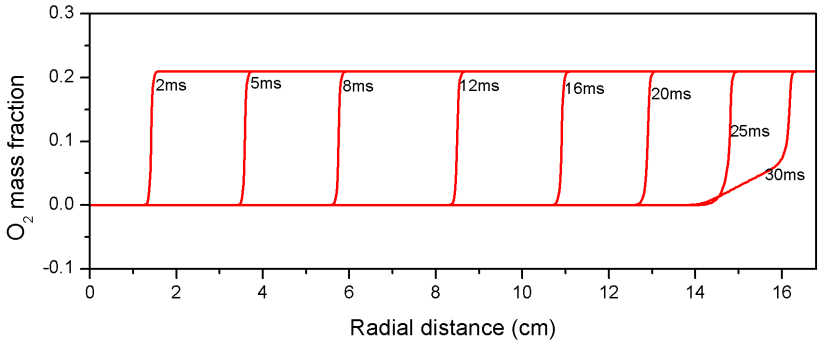


(e)

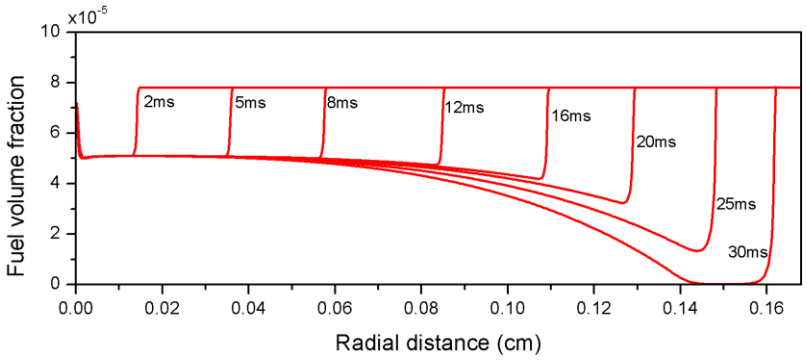


(f)

Figure 2: Flame properties of alloy dust explosion in the 20-L sphere

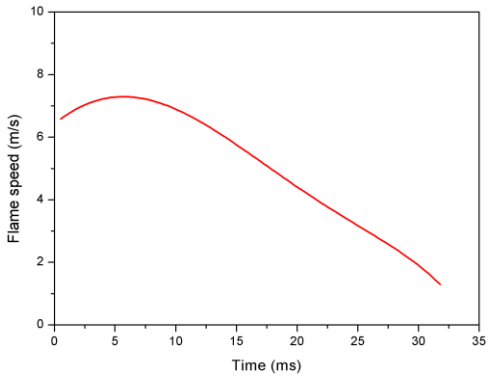

Figure 3: Flame speed in the explosion process

*4.2. Alloy dust explosion properties*

This section will present a preliminary study of the alloy dust explosion. Since the experimental tests are still in progress, a preliminary comparison of the modeling effort is made and more data will be produced in the future for a detailed study. The explosion experiment is carried out with an unscreened alloy sample ranging from 20μm to 500μm at a mass concentration of 1000g·m-3 in a standard 20-L spherical testing chamber. The powder sample is injected from a compressed container into the pre-evacuated chamber at a gauge pressure of –0.6bar prior to ignition. Pressure starts to rise after ignition of the dust cloud and is then recorded continuously by the pressure sensor until the end of the explosion, see the blue line with hollow circles in Fig.4 and Fig 5. Two important points corresponding to the peak pressure (denoted by +) and the maximum pressure rising rate (denoted by *) are identified by a post-processing software respectively for further information of Pmax and Kst.

Table 2 Calibrated model parameters for alloy dust explosion

| Kinetic models | Parameters |
|---|---|
| Kinetic model I | $A$=3.8×10$^{4}$ |
| | $E$=5×10$^{7}$J·kmol$^{-1}$ |
| | $f$=0.95 |
| Kinetic model II | $K$=1.6×10$^{4}$s·m$^{-2}$ |
| | $T_{ig}$=600K |
| | $f$=0.95 |

The alloy is not a simple blend of different metals, chemical bonding and lattice structure will have great effect on the combustion features. Therefore, a simple heat loss factor might be invalid to account for the complex dissociation reactions. In addition, a detailed combustion mechanism might be more suitable than the current lumped single-step model, but this will pose great challenges to the numerical modelling. For the sake of simplicity, no new features are added to the model in the current stage. The explosion model with calibrated kinetic parameters is used to simulate this process at the same condition of the experiment. These calibrated parameters were obtained from a parametric study and given in Table 2. Thermal properties of the metal components and their corresponding oxides used in the simulation are given in Table 3 and Table 4, respectively. Results obtained with kinetic method I and kinetic method II are compared against experimental tests in Fig.4 and Fig 5, respectively. It can be noted that overpressure can be well predicted by the current explosion model either with kinetic method I or kinetic method II, provided that the model parameters can be carefully calibrated. However, the detailed evolutions of the overpressure predicted by the two kinetic methods are slightly different. The best performance of the current model is achieved when combined with kinetic method I that the predicted pressure history which almost overlaps with that measured by the experiment. The corresponding deflagration index predicted by this simulation is therefore very close to the experimental value, which are 59.4 and 63.8, respectively. In contrast, the kinetic method II does not

capture the pressure history that well. Thus, the predicted deflagration index is underestimated by about 38%.

Table 3 Physical properties of the metal components

| Metal | Mw(kg/kmol) | $T_{bp}$(K) | $T_{mp}$(K) | $\Delta H_{vol}$(kJ/mol) | $\Delta H_{mel}$() |
|---|---|---|---|---|---|
| Ti | 47.867 | 3560 | 1941 | 425 | 18.7 |
| Zr | 91.224 | 4682 | 2128 | 580 | 21 |
| Mn | 54.938 | 2334 | 1519 | 220 | 13.2 |
| Cr | 51.996 | 2944 | 2180 | 339 | 20.5 |
| Fe | 55.845 | 3134 | 1811 | 347 | 13.8 |

Table 4 Physical properties of the metal oxides

| Oxide | Mw(kg/kmol) | $T_{vol}$(K) | $\Delta H_{f,298}$(kJ/mol) | $\Delta H_{vol}$(kJ/mol) | $H_{Tvol}$-$H_{298}$+$\Delta H_{vol}$(kJ/mol) |
|---|---|---|---|---|---|
| $Ti_3O_5$ | 223.598 | 4000 | -2459 | 1890 | 2970 |
| $ZrO_2$ | 123.223 | 4280 | -1097 | 920 | 1320 |
| $Mn_3O_4$ | 228.812 | 3120 | -1388 | - | 1005* |
| $Cr_2O_3$ | 151.990 | 3280 | -1135 | 1160 | 1700 |
| FeO | 71.844 | 3400 | -272 | 610 | 830 |

*Inaccurate

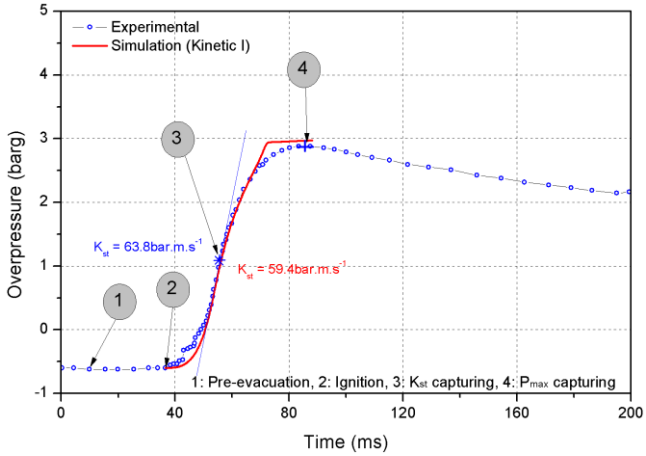


Figure 4 Pressure history of the alloy dust explosion in the 20L- sphere – a comparison of the explosion model with kinetic method I and experimental data

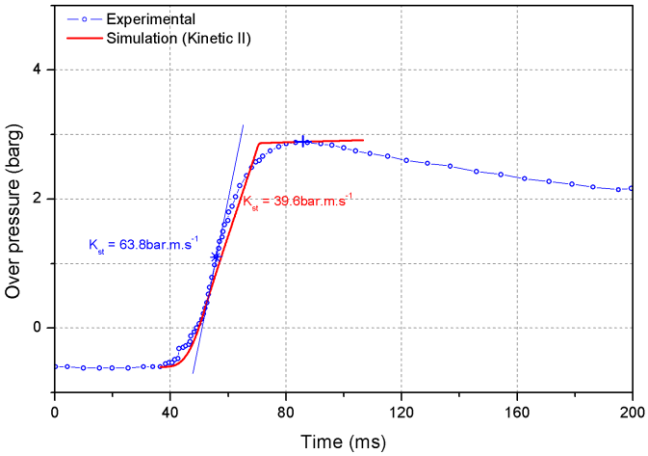


Figure 5 Pressure history of the alloy dust explosion in the 20L- sphere – a comparison of the explosion model with kinetic method II and experimental data

## 5. Conclusions

A 1-D explosion model has been developed in this paper to simulate the flame propagation of a metal dust cloud in a 20L-spherical chamber. In the model transport equations of energy, species and solid volume fraction are solved numerically. Velocity field of the gas phase and pressure within the chamber are calculated by integrating the continuity equation. Density of the gas phase is updated using the ideal gas equation of state. This model is referred to as a quasi-two-phase approach as compared with the work conducted by Ogle who employed a single-phase model to approximate the two-phase process. Momentum equation of the solid particles is not solved in this study so that the complex interaction between the solid and the gas phase is ignored. A lumped single-step combustion mechanism is used in the current explosion model. Then, two kinetic methods are used to calculate the combustion rate of the particles. The model is applied to simulate the explosion process of the alloy powder used for hydrogen storage. The results show correct behavior of velocity, density, temperature and other important variable in the explosion process. Two kinetic models have been tested for dust combustion and compared with experimental data. Kinetic method I appears to be more suitable to describe the metal dust explosion in terms of prediction of the pressure history. Although this is only a preliminary study, the results derived in this work will be of great significance for the safety assessment of the alloy powder in the process of fabrication, storage and transportation. Further work will be done with more detailed testing of the alloy dust explosions. Comprehensive reaction mechanism for both combustion and dissociation will be considered as well in the future to enhance the performance of the model.

## 6. References


[1] S.A. Sherif, D.Y. Goswami, E.L. Stefanakos, A. Steinfeld, Handbook of Hydrogen, CRC Press, 2014.

[2] M. Ni, M.K.H. Leung, D.Y.C. Leung, K. Sumathy, A review and recent developments in photocatalytic water-splitting using TiO2 for hydrogen production, Renew. Sustain. Energy Rev. 11 (2007) 401–425. doi:10.1016/j.rser.2005.01.009.

[3] C. Corgnale, B. Hardy, T. Motyka, R. Zidan, J. Teprovich, B. Peters, Screening analysis of metal hydride based thermal energy storage systems for concentrating solar power plants, Renew. Sustain. Energy Rev. 38 (2014) 821–833. doi:10.1016/j.rser.2014.07.049.

[4] E. David, An overview of advanced materials for hydrogen storage, J. Mater. Process. Technol. 162-163 (2005) 169–177. doi:10.1016/j.jmatprotec.2005.02.027.

[5] A. Zuttel, Materials for hydrogen storage, Mater. Today. 6 (2003) 24–33. doi:10.1016/S1369-7021(03)00922-2.

[6] T. Tanaka, M. Keita, D.E. Azofeifa, Theory of hydrogen absorption in metal hydrides, Phys. Rev. B. 24 (1981) 1771–1776. doi:10.1103/PhysRevB.24.1771.

[7] B. Sakintuna, F. Lamari-Darkrim, M. Hirscher, Metal hydride materials for solid hydrogen storage: A review, Int. J. Hydrogen Energy. 32 (2007) 1121–1140. doi:10.1016/j.ijhydene.2006.11.022.

[8] S. Kumar, A. Jain, T. Ichikawa, Y. Kojima, G.K. Dey, Development of vanadium based hydrogen storage material: A review, Renew. Sustain. Energy Rev. 72 (2017) 791–800. doi:10.1016/j.rser.2017.01.063.

[9] G. Marbán, T. Valdés-Solís, Towards the hydrogen economy?, Int. J. Hydrogen Energy. 32 (2007) 1625–1637. doi:10.1016/j.ijhydene.2006.12.017.

[10] E. Veleckis, R.K. Edwards, Thermodynamic properties in the systems vanadium-hydrogen, niobium-hydrogen, and tantalum-hydrogen, J. Phys. Chem. 73 (1969) 683–692. doi:10.1021/j100723a033.

[11] S. Kumar, M. Taxak, N. Krishnamurthy, Synthesis and hydrogen absorption kinetics of V4Cr4Ti alloy, J. Therm. Anal. Calorim. 112 (2013) 51–57. doi:DOI 10.1007/s10973-012-2643-5.

[12] J.C. Crivello, R. V. Denys, M. Dornheim, M. Felderhoff, D.M. Grant, J. Huot, T.R. Jensen, P. de Jongh, M. Latroche, G.S. Walker, C.J. Webb, V.A. Yartys, Mg-based compounds for hydrogen and energy storage, Appl. Phys. A Mater. Sci. Process. 122 (2016) 1–17. doi:10.1007/s00339-016-9601-1.
[13] M. Bououdina, J.. Soubeyroux, P. de Rango, D. Fruchart, Phase stability and neutron diffraction studies of the laves phase compounds Zr(Cr1-xMox)2 with 0.0<x<0.5 and their hydrides, Int. J. Hydrogen Energy. 25 (2000) 1059–1068. doi:10.1016/S0360-3199(99)00087-7.
[14] E. Akiba, H. Iba, Hydrogen absorption by Laves phase related BCC solid solution, Intermetallics. 6 (1998) 461–470. doi:10.1016/S0966-9795(97)00088-5.
[15] M. Hirscher, Handbook of hydrogen storage: New Materials for Future Energy Storage, WILEY-VCH Verlag GmbH & Co. KGaA, 2009.
[16] E.I. Gkanas, D.M. Grant, M. Khzouz, A.D. Stuart, K. Manickam, G.S. Walker, Efficient hydrogen storage in up-scale metal hydride tanks as possible metal hydride compression agents equipped with aluminium extended surfaces, Int. J. Hydrogen Energy. 41 (2016) 10795–10810. doi:10.1016/j.ijhydene.2016.04.035.
[17] R.K. Eckhoff, Understanding dust explosions. The role of powder science and technology, J. Loss Prev. Process Ind. 22 (2009) 105–116. doi:10.1016/j.jlp.2008.07.006.
[18] R.K. Eckhoff, Current status and expected future trends in dust explosion research, J. Loss Prev. Process Ind. 18 (2005) 225–237. doi:10.1016/j.jlp.2005.06.012.
[19] B. Seth, S.K. Aggarwal, W.A. Siringnano, Flame Propagation Through an Air-Fuel Spray Mixture With Transient Droplet Vaporization., Combust. Flame. 39 (1980) 149–168. doi:10.1016/0010-2180(80)90014-0.
[20] S.K. Aggarwal, W.A. Sirignano, Unsteady spray flame propagation in a closed volume, Combust. Flame. 62 (1985) 69–84. doi:10.1016/0010-2180(85)90094-X.
[21] G. Continillo, W.A. Sirignano, Numerical study of multicomponent fuel spray flame propagation in a spherical closed volume, Symp. Combust. 22 (1989) 1941–1949. doi:10.1016/S0082-0784(89)80209-7.
[22] G. Continillo, Numerical Study of Coal Dust Explosions in Spherical Vessels., Am. Chem. Soc. (1988) 188–196.
[23] A. Di Benedetto, P. Russo, Thermo-kinetic modelling of dust explosions, J. Loss Prev. Process Ind. 20 (2007) 303–309. doi:10.1016/j.jlp.2007.04.001.
[24] A. Di Benedetto, P. Russo, P. Amyotte, N. Marchand, Modelling the effect of particle size on dust explosions, Chem. Eng. Sci. 65 (2010) 772–779. doi:10.1016/j.ces.2009.09.029.
[25] K.L. Cashdollar, M. Hertzberg, 20-L Explosibility Test Chamber for Dusts and Gases, Rev. Sci. Instrum. 56 (1985) 596–602. doi:10.1063/1.1138295.
[26] K.L. Cashdollar, Overview of dust explosibility characteristics, J. Loss Prev. Process Ind. 13 (2000) 183–199. doi:10.1016/S0950-4230(99)00039-X.
[27] ISO, Explosion protection systems-Part 1: determination of explosion indices of combustible dusts in air, 1985.
[28] R.A. Ogle, L.D. Chen, J.K. Beddow, P.B. Butler, An Investigation of Aluminum Dust Explosions, Combust. Sci. Technol. 61 (1988) 75–99. doi:10.1080/00102208808915758.
[29] R.A. Yetter, G.A. Risha, S.F. Son, Metal particle combustion and nanotechnology, Proc. Combust. Inst. 32 II (2009) 1819–1838. doi:10.1016/j.proci.2008.08.013.
[30] K. Benkiewicz, A.K. Hayashi, Aluminum dust ignition behind re ected shock wave: two-dimensional simulations, Fluid Dyn. Res. 30 (2002) 269–292.